Processing and Properties of Eu^{3+}-doped Transparent YAG ($Y_3Al_5O_{12}$) Nano Glass-Ceramics

Anal Tarafder, Atiar Rahaman Molla, and Basudeb Karmakar†

Glass Science and Technology Section, Glass Division,
Central Glass and Ceramic Research Institute
(Council of Scientific and Industrial Research), Kolkata 700032, India

Abstract

Eu^{3+}-doped novel mother glass in the K_2O-SiO_2-Y_2O_3-Al_2O_3 (KSYA) system was prepared by the melt-quench technique. The transparent $Y_3Al_5O_{12}$ (YAG) glass-ceramics were derived from this glass by a controlled crystallization process. The formation of YAG crystal phase, size and morphology with progression of heat-treatment was examined by X-ray diffraction (XRD), transmission electron microscopy (TEM), field emission scanning electron microscopy (FESEM) and Fourier transformed infrared reflectance spectroscopy (FT-IRRS). The crystallite sizes obtained from XRD are found to increase with heat-treatment time and vary in the range 35-45 nm. The photoluminescence spectra of Eu^{3+} ions exhibit emission transitions of $^5D_{0,1} \rightarrow {}^7F_j$ (j = 0, 1, 2, 3 and 4) and its excitation spectra shows a charge transfer band (CTB) around 280 nm. From these emissions, the site symmetry in the vicinity of Eu^{3+} ions has been found to be C_s or lower than C_s in the nano glass-ceramics. The absorption and fluorescence spectra reveal that the Eu^{3+} ions are entering into the YAG nanocrystals of the glass-ceramics. The present study indicates that the incorporation of Eu^{3+} ions into YAG crystal lattice enhance the fluorescence performance of the nano glass-ceramics. We believe that this work would generate new avenues in the exploration of YAG nano glass-ceramics in particular and other glass-ceramics of very high temperature melting crystals in general.

†Author to whom correspondence should be addressed.
e-mail address: basudebk@cgcri.res.in

I. Introduction

Optically transparent single crystal YAG is used as optical host materials in various solid-state lasers for its outstanding optical properties when doped with lanthanide ($4f^{1-13}$) or transition ($3d^{1-9}$) elements. Laser operation of Nd:YAG was first demonstrated by Geusic et al.[1] at Bell Laboratories in 1964. Since then it is one of the most widely used laser materials available till date. YAG based materials are used for many different applications such as in cathode-ray tube (CRTs), field emission displays (FED), scintillation, phosphors and electro-luminescent applications as well.[2-7] Generally, single crystals YAG is formed by the crystal growth techniques. Single crystal YAG preparation by crystal growth technique is expensive and requires very sophisticated equipment, and is technically difficult to produce in desired shape, size and optical quality.

In addition to its single crystal form, polycrystalline YAG doped with active rare-earth (RE) ions prepared by different routes other than glass-ceramics route has received much attention and has been used as an excellent phosphor or laser material.[8-12] However, the glass-ceramics route has not been used to prepare YAG based transparent glass-ceramics laser materials due to several difficulties such as requirement of very high temperature (> 1650^{o}C) and opaqueness of the resultant product. Johnson et al.[13] investigated kinetics and pathways for crystallization of glasses with YAG. Nishi et al.[14] investigated the phase-selective cathodoluminescence spectra of Er:YAG glass-ceramics. Crystallization of YAG in yttrium alumina silica glass was reported by P. Jander[15] and found that the crystallized phase was almost YAG but not transparent or nanocrystalline. It was also observed that the batch materials could not be melted completely and unmelted batch materials remained at the bottom of the melting crucible. Therefore, the reports of YAG based transparent glass-ceramics prepared by controlled crystallization of melt-quenched mother glass obtained from

a homogeneous glass melt are very rare. Moreover in all the cases the derived glass-ceramics are macrocrystalline in nature and not suitable for optical applications.

During the past decades, the novel and enhanced properties of nanostructured materials have also attracted considerable attention for their interesting optical properties.[16, 17] In this context Tarafder el al.[18] and Chaliha et al.[19] have very recently reported the processing and properties of RE-doped nanostructured transparent glass-ceramics prepared by controlled crystallization technique. They have also reported that those nano glass-ceramics have potential optical applications. To the best of our knowledge, there is no report on transparent nanostructured YAG glass-ceramics in the potassium aluminosilicate, K_2O-SiO_2-Y_2O_3-Al_2O_3 (KSYA) glass-matrix due to the difficulties in preparation of transparent precursor glass in general and transparent glass-ceramics in particular which involves high temperature (about 1650-1700^oC) for its precursor glass melting. In view of this, it is interesting to study the properties of nanostructured YAG glass-ceramics prepared by controlled crystallization of mother glass.

In the present work, we report the preparation of Eu^{3+}-doped novel K_2O-SiO_2-Y_2O_3-Al_2O_3 (KSYA) based glass by melt-quench technique and transparent nano glass-ceramics by isothermal controlled crystallization of mother glasses. The crystallization process has been studied by differential thermal analysis (DTA), X-ray diffraction (XRD), transmission electron microscopy (TEM), field emission scanning electron microscopy (FESEM) and Fourier transform infrared reflection spectroscopy (FT-IRRS). The glass and derived nano glass-ceramics were characterized by studying their thermal, structural and optical properties.

II. Experimental Procedure

(1) Mother Glass Preparation

The mother glass having molar composition $28Ki_2O$-$42SiO_2$-$11.25Y_2O_3$-$18.75Al_2O_3$ doped with Eu_2O_3 (0.5 mol% in excess) was prepared from pure raw materials such as potassium carbonate, K_2CO_3 (GR, 99%, Loba Chemie, Mumbai, India), silica, SiO_2 (99.8%, Sipur A1 Bremtheler Quartzitwerk, Usingen, Germany), yttrium (III) oxide, Y_2O_3 (99.99%, Alfa Aesar, Ward Hill, MA), alumina, Al_2O_3 (99%, Aldrich, Milwaukee, WI), and europium (III) oxide, Eu_2O_3 (99.9%, Alfa Aesar, Ward Hill, MA) by conventional melt-quench technique. The well-mixed batch of about 150 g glass was melted in a platinum crucible in an electric furnace at 1680°C for 2h in air with intermittent stirring. The glass melt was poured onto a pre-heated iron mould. It was annealed at 700°C for 2 h to remove the internal stresses of the glass and then slowly cooled down to room temperature. The as-prepared glass block was cut into desired dimensions and optically polished for ceramization and subsequent characterization.

(2) Characterization

The density of mother glass was measured using Archimedes principle using water as buoyancy liquid. The refractive indices were measured by a Prism Coupler (Model: 2010/M, Metricon Corporation, Pennington, NJ) at five different wavelengths (λ = 473, 532, 633, 1064 and 1552 nm). Differential thermal analysis (DTA) of mother glass powder was carried out up to 1100^{o}C from room temperature at the rate of 8^{o}C/min with a SETARAM instrument (Model: TG/DTA 92, SETARAM Instrumentation, Caluire, France) to determine the crystallization peak temperature (T_P). The coefficient of thermal expansion (CTE), glass transition temperature (T_g) and dilatometric softening temperature (T_d) of the mother glass of cylindrical test sample (φ = 6 mm, L = 25 mm) was measured with an accuracy of ±1% using

a horizontal-loading dilatometer (Model: DIL 402 PC, NETZSCH-Gerätebau GmbH, Selb, Germany) after calibration with a standard alumina supplied with the instrument by the manufacturer. The CTE in the temperature range 50-350^{o}C is reported here. XRD patterns were recorded using an XPERT-PRO MPD diffractometer (PANalytical, Almelo, the Netherlands) and the measurements were operated with Ni-filtered CuK_{α} = 1.5406 Å radiation as the X-ray source at 40 kV and 40 mA to identify the developed crystalline phases. The 2θ scan range was 10^{o} to 80^{o} with a step size of 0.05^{o}.

The TEM images and selected area electron diffraction (SAED) pattern of powdered glass-ceramics were obtained from FEI (Model: Tecnai G^2 30ST, FEI Company, Hillsboro, OR) instrument. A high resolution FESEM (Gemini Zeiss Supra^{TM} 35 VP model of Carl Zeiss Microimaging GmbH, Berlin, Germany) was used to observe the microstructure of freshly fractured surfaces of the heat-treated nano glass-ceramics after etching in 2% HF aqueous solution for 5 minutes, dried and then coated with a thin carbon film. The FTIR reflectance spectra of all Eu^{3+}-doped glass and glass-ceramics were recorded using a FTIR spectrometer (Model: 1615 Series, Perkin-Elmer Corporation, Norwalk, USA) in the wavenumber range 400-1500 cm^{-1} with a spectral resolution of $\pm$ 2 cm^{-1} and at 15^{o} angle of incidence. Optical absorption spectra were recorded UV-Vis-NIR spectrophotometer (Lambda 20, Perkin-Elmer Corporation, Norwalk, USA) at room temperature to monitor the changes of the environmental structure of the Eu^{3+} ions. The fluorescence emission and excitation spectra were measured on a bench top modular spectrofluorometer (QuantaMaster, Photon Technology International, Birmingham, NJ) attached with a Xe arc lamp as excitation source. The excited state lifetime was measured with the same instrument using a Xe flash lamp of 75 W.

III. Results and Discussion

(1) Thermal, Optical and Other Physical Properties

The composition of mother glass is $28Ki_2O$-$42SiO_2$-$11.25Y_2O_3$-$18.75Al_2O_3$ (mol%) doped with 0.5 mol% Eu_2O_3 (in excess). We tried to melt several glass compositions with higher quantities of YAG forming oxides (Y_2O_3 and Al_2O_3). It was observed that higher quantity (>30 mol%) of Y_2O_3 and Al_2O_3 could not be incorporated in the glass matrix without sacrificing the transparency. In this context, it may be mentioned that Nishi et al.[14] could incorporate 29.5 mol% YAG compositions in the $34CaO$-$8.5Y_2O_3$-$21Al_2O_3$-$36SiO_2$-$0.5Er_2O_3$ glass-matrix. However, their ultimate glass-ceramic was opaque. The DTA curve of the mother glass is shown in Fig. 1. It exhibits two intense exothermic peak at 940^oC (T_{p1}) and 971^oC (T_{p2}) corresponding to the YAG and potassium aluminium silicate, $KAlSiO_4$ crystallization respectively. In addition the T_g estimated from this curve found to be 821^0C. Coefficient of thermal expansion (CTE), glass transition temperature (T_g) and dilatometric softening point (T_d) of the mother glass were measured using a dilatometer and the measured values from this dilatometric curve (Fig. 2) are presented in Table I. CTE was measured over the temperature range of 50- 350^0C and its value is 111 x 10^{-7} K^{-1}. The dilatometric curve revealed that the mother glass possesses a very high glass transition (819^0C) and softening temperature (867^0C) due to the presence of high melting SiO_2, Y_2O_3 and Al_2O_3 as major constituents of glass.

The mother glass is visually transparent, appearing light brownish yellow due to Eu^{3+} doping. The mother glass samples were heat treated at 750^oC for 0, 3, 10, 30 and 50 h after nucleating at 700^oC for 2 h. The obtained samples were labelled as a, b, c, d and e (Fig. 3) respectively for convenience. In the preliminary experimentation to obtain nanostructured transparent glass-ceramics, it was observed that the mother glass had been transformed into opaque glass-ceramics after heat-treating at T_g or above T_g. In the course of this investigation,

we established an optimum nucleation temperature of 700°C and crystallization temperature of 750°C where the nano glass-ceramics maintain their transparency. Tarafder et al.[20] has also adopted a similar heat-treatment protocol for developing nanostructured transparent Eu^{3+}:$LiTaO_3$ in Li_2O-Ta_2O_5-SiO_2-Al_2O_3 glass-ceramics. The transparency of the mother glass persists in the heat-treated samples. The glass-ceramics thus obtained became more transparent by decreasing the brownish yellow color intensity due to devitrification with the progress of heat-treatment duration. The measured density of the mother glass is 3.033 $g.cm^{-3}$ and this high value attributes to the presence of relatively high molecular weight Y_2O_3 as a component of the glass. Fig. 4 presents Cauchy fitting based on measured refractive indices at five different wavelengths (see experimental techniques) and shows the dependences of the refractive index on the wavelength for mother glass (a) and the 30 h heat-treated glass-ceramics (d) sample. In general, refractive index decreases with increasing wavelength due to dispersion. This trend is observed in both the samples. In addition to this, the refractive index of the glass-ceramic sample (d) has increased in comparison with mother glass (a) that can be seen in Fig. 4. The refractive indices n_F, n_D and n_C have been estimated at three standard wavelengths (λ_F = 486.1 nm, λ_D = 589.2 nm and λ_C = 656.3 nm respectively) from the dispersion curve (Fig. 4, curve a). The Abbe number (υ_D) is calculated by the relation

$$\upsilon_D = \frac{n_D - 1}{n_F - n_C} \qquad (1)$$

The calculated υ_D for mother glass (a) and glass-ceramic (d) are 53 and 56 respectively. Therefore, the glass-ceramics are of lower dispersion than mother glass. From the measured glass density (ρ) and refractive index (n_D) at wavelength λ_D = 589.2 nm, other related optical properties have been determined using relevant expressions and the results are presented in Table I. It is observed that the formation of high refractive index YAG (RI = 1.8317 at 600

nm[21]) causes the heat-treated sample to exhibit higher refractive indices as compared to mother glass. This is shown in Fig. 4, curve-d.

(2) X-ray Diffraction Analysis

The X-ray diffraction pattern of the Eu^{3+}-doped KSYA mother glass and cerammed glass-ceramics are shown in Fig. 5. No diffraction peak appears for the samples a-c which indicates that the powders are amorphous in nature for these samples. The diffraction peak of the samples d and e heat-treated for longer duration are indexed and it resembled to some extent as $Y_3Al_5O_{12}$ phase (JCPDS file 33-0040). Progression of heat-treatment leads to an increase of diffraction peak intensity and a decrease of peak full-width at half-maxima (FWHM) due to the improved crystallinity and the coarsening of grains. The two YAG glass-ceramics obtained after heat-treating the mother glass at 940 and 980^0C for 10 h duration are opaque in appearance and their respective XRD patter is included in Fig. 5. The sharp diffraction lines are also attributed to the better crystallinity and coarsening of grains in the opaque YAG glass-ceramics.

From the full width at half maximum (FWHM) of the most intense diffraction peak (420) of transparent YAG nano glass-ceramics, the average crystallite size (diameter, *d*) is calculated by using the Scherrer's formula[22]

$$d = 0.9\lambda / \beta \cos\theta \qquad (2)$$

where λ is the wavelength of X-ray radiation (CuK_α = 1.5406Å), and β is the full width at half maximum (FWHM) of the peak at 2θ.

The average calculated crystallite sizes of YAG nanocrystal increase with progression of heat-treatment and the values increasing in the range 35-45 nm over the investigated heat-treatment time period. It is observed from the XRD patterns that there is evidence of presence of minor amount $KAlSiO_4$ (JCPDS file 33-0989) in the derived nano glass-ceramics which is

also marked in Fig. 5. It correlates well with the observation of formation of minor spodumene ($LiAlSi_2O_6$) phase in the Eu^{3+}:Li_2O-Ta_2O_5-SiO_2-Al_2O_3 system as reported by Tarafder et al.[18]

(3) TEM and FESEM Image Analyses

TEM and FESEM analyses were performed to study the size, shape and morphology of nano glass-ceramics. Fig. 6 shows bright field TEM image of nano glass-ceramics (e) and its inset shows the selected area electron diffraction (SAED) pattern from the dotted encircled region. The SAED pattern confirms the presence of crystalline YAG in the nano glass-ceramics as JCPDS file 33-0040. It is also found that the crystallite sizes are in the range of 10-15 nm. FESEM images of the fractured surface of samples c and e have been presented in Figs. 7(a) and (b) respectively. From the FESEM micrographs, it is clearly observed that the glassy matrix of the heat-treated samples initially phase separated on nanometric scale followed by incipient precipitation of defined crystallites (YAG) within the phase-separated grains (Fig. 7 a) with increase in heat-treatment time. The phase separated grains are irregular in shapes and distributed uniformly thought out the bulk glass matrix. The size of the phase separated grains varies in the range 50-60 nm. These grains are well separated and grown with distinct features by way of further increase in heat-treatment time (Fig. 7 b). Comparing with the crystalline sizes, it is clear that these phase separated grains are polycrystalline in nature. The crystallite sizes obtained from TEM image is less than that of evaluated by Scherrer's formula using XRD patterns. This difference is due to the following facts. TEM gives the images of crystallites at a particular selected region of the sample whereas Scherrer's formula gives the average crystallite sizes comprising of from very small to very large size crystallites. This difference, therefore, is not unexpected.

(4) Fourier Transform Infrared Reflectance Spectroscopy (FTIRRS)

The FTIR reflectance spectra of the bulk mother glass and heat-treated samples in the wavenumber range 400-1500 cm^{-1} are shown in Fig. 8(A). It is seen from these spectra that the mother glass (curve-a) exhibits three broad reflection bands centred around 950, 675 and 475 cm^{-1} as a result of wider distribution of silicon and YAG structural units. It is also observed that one more reflection band gradually appeared around 575 cm^{-1} with increasing heat-treatment duration. The reflection bands centred at 690, 575 and 475 cm^{-1} are assigned to the characteristics Al-O and Y-O bond vibrations of crystalline YAG. All these bands well matched with the reported data of a crystallized YAG.[23-26] The reflection band centred at 950 cm^{-1} and gradually shifted to 980 cm^{-1}. It is assigned to Si-O stretching vibration of residual glass and potassium aluminium silicate.[27] It is seen that with progression of heat-treatment all the FTIR reflection band intensities (here reflectivities) increase and become narrower gradually. The values of FTIR band intensities due to YAG formation at 690 and 475 cm^{-1} are given in Table II and plotted in Fig. 8(B) with heat-treatment time. Thus from the investigations of FTIR reflectance spectra of Eu^{3+} doped K_2O-SiO_2-Y_2O_3-Al_2O_3 glass and glass-ceramics, it is clear that the crystallization is taking place with initial phase separation followed by advancement of mainly YAG crystal formation along with minor quantity of potassium aluminium silicate phase formation in the residual glass matrix. The results of the FTIRRS are in good agreement with that of XRD, TEM and FESEM studies.

(5) UV-Visible Absorption Spectra

The room temperature measured absorption spectra of Eu^{3+}-doped KSYA mother glass and heat-treated glass-ceramic samples in the UV-visible range (350-600 nm) have been presented in Fig. 9. The spectra reveal the absorption bands of Eu^{3+} ion due to transitions from its ground state multiplets such as $^7F_0$ and thermally populated $^7F_1$ levels to the upper

levels of $4f^6$ configuration. In the case of Eu^{3+} ions, the ground state $^7F_0$ and the higher-level $^7F_1$ are very close to each other (around 360 cm^{-1} apart). So, at room temperature a significant amount of $^7F_1$ level is thermally populated[28, 29] according to Boltzmann distribution law with the thermal energy kT (0.025 eV = 201.6 cm^{-1} at room temperature which results in a characteristic absorption spectrum of Eu^{3+} ions exhibiting closely spaced doublets. In the present study, the recorded absorption peaks for all the glass and glass-ceramics under investigation are assigned in accordance with Carnall's convention.[28] The observed transitions of $^7F_0 \rightarrow {}^5D_0$ (578 nm), $^5D_1$ (526 nm), $^5D_2$ (463 nm), $^5D_3$ (412 nm), $^5L_6$ (393 nm), $^5G_2$ (381 nm), $^5G_4$ (376 nm), $^5D_4$ (362 nm) and $^7F_1 \rightarrow {}^5D_1{}^*$ (531 nm), $^5L_6{}^*$ (401 nm) are marked in the absorption spectra depending upon their peak energies. From this figure it is noticed that the base line of absorption spectra of heat-treated samples (c-e) has been elevated significantly with the diminishing intensities of the absorption peaks. This elevation could be attributed to scattering of short wavelength light by the crystals[30, 31] or may be due to the difference in refractive index of crystalline phase (RI of YAG is 1.8317 at 600 nm[21] with that of residual glassy matrix (RI = 1.5905 at 656.3 nm, see Table I). These elevations are larger in lower wavelength region than that of higher wavelength. Since the crystallites (35-45 nm) are smaller than the visible wavelength, a Rayleigh scattering model should be applicable.[32] According to this model, the scattering loss, τ is given by

$$\tau = \frac{32\pi^4 d^3 (n\Delta n)^2}{3\lambda^4} NV \qquad (3)$$

where d is the particle diameter, λ the wavelength of light, n the refractive index, N the number density of particles, and V the volume of the particle. In general, with progression of heat-treatment, the number and sizes of nanocrystallites developed in the glassy matrix have been increased. Hence the scattering centres and scattering loss have also been increased that

corresponds to a decrease in the visible transparency of the nano glass-ceramics. The similar type elevation of base line of absorption spectrum in nano glass-ceramics has earlier been shown by Hirano et al.[33] However, there is no significant difference amongst the shapes (profiles) of the absorption bands of the glass and nano glass-ceramics.

(6) Emission Spectra

The emission spectra of the mother glass and the glass-ceramics under the excitation at 396 nm monochromatic light from an arc Xe lamp is shown in Fig. 10. The spectra of the Eu^{3+}-doped glass and the glass–ceramics exhibit five emission peaks at 579, 592, 613, 653 and 704 nm. These five emission peaks can be attributed to the $^5D_0 \rightarrow {}^7F_{0,\,1,\,2,\,3,\,4}$ transitions of Eu^{3+}. More emission peaks have been observed in YAG nano powder[34-36] in comparison to our developed nano glass-ceramics because of the formed YAG nanocrystals are surrounded by amorphous glass matrix which leads to less emission peaks. The main emission peak near 613 nm is assigned to the induced electric dipole (ED) transition $^5D_0 \rightarrow {}^7F_2$ of Eu^{3+} and it is dominant over emission peak near 592 nm which is assigned to the magnetic dipole (MD) transition $^5D_0 \rightarrow {}^7F_1$ of Eu^{3+}. The induced electric dipole transition appears when Eu^{3+} ions occupy non-centrosymmetric lattice centres, whereas the magnetic dipole transition appears due to both centrosymmetric and non-centrosymmetric lattice centres.[37] Therefore, the analysis of the spectral features of $^5D_0 \rightarrow {}^7F_{1,2}$ transitions are very important to understand the local environment of Eu^{3+} ions. Upon the heat-treatment, it is also observed that the emission transitions from $^5D_0 \rightarrow {}^7F_1$ (MD) and $^5D_0 \rightarrow {}^7F_2$ (ED) in glass-ceramic samples (b-e) have displayed three and five Stark splittings respectively. These changes in emission spectra of glass-ceramics suggest the fact that the Eu^{3+} ions enter into the crystalline phase (YAG) thus formed. The Eu^{3+} ion is entering into the crystal (YAG) and it prefers to replace Y^{3+} over Al^{3+} site due to the closeness of their ionic radii (Eu^{3+} = 0.95 Å, Y^{3+} = 1.04 Å and Al^{3+} = 0.50

Å). Following the crystal field selection rules, the presence of $^5D_0 \rightarrow {}^7F_0$ transition and the existence of three and five Stark components for the transitions $^5D_0 \rightarrow {}^7F_1$ and $^5D_0 \rightarrow {}^7F_2$ (see inset of Fig. 10) respectively, this could be suggested that the rare earth (Eu^{3+}) ions are facing near C_s or lower point symmetry in its vicinity in this host matrix.[37, 38] As seen in Fig. 9, the $^5D_0 \rightarrow {}^7F_2$ transition is dominant among the $^5D_0 \rightarrow {}^7F_J$ transitions, and the half width for the $^5D_0 \rightarrow {}^7F_2$ transition is about 10 nm. It is, therefore, revealed from the emission spectra that the crystal field at Eu^{3+} sites in transparent nanocrystalline glass-ceramic composites is not homogeneous. The local field asymmetry defining factor such as relative intensity ratio of I_{ED} to I_{MD} of Eu^{3+} doped glass and nano glass-ceramics has been estimated from their fluorescence spectra and listed in Table II. The values of 5.109 for mother glass, and of 4.895, 4.821, 4.265 and 3.593 for the nano glass-ceramics (b-e) were obtained. A similar type observation has also been reported in transparent TeO_2-based glass-ceramics by Hirano et al.[33] The asymmetric ratio of all the samples is greater than unity, which implies that the Eu^{3+} ions take non-centrosymmetric sites.

(7) Excitation Spectra

The fluorescence excitation spectra of samples (a) and (e) are measured in the wavelength range 250 – 575 nm by monitoring with the intense red emission located at 613 nm. The excitation spectra (Fig. 11) give a vivid picture of the presence of charge transfer band (CTB) of Eu^{3+} and different f-f transitions within Eu^{3+} $4f^6$ configuration. The excitation spectra consist of two intense bands at 396 and 466 nm in addition to eight relatively weak bands peaking about 300, 322, 364, 383, 404, 416, 528 and 534 nm. The bands peaking around 322, 364, 396, 466 and 528 nm are assigned to transitions from the $^7F_0$ level to the $^5H_4$, $^5D_4$, $^5L_6$, $^5D_3$, $^5D_2$, and $^5D_1$ levels of f-f transitions of Eu^{3+} ions respectively. On the other hand, rest of the bands peaking around 300, 383, 404, 416 and 534 nm are assigned to the transitions from

thermally populated $^7F_1$ level to the $^5F_4$, $^5L_7$, $^5L_6$, $^5D_3$ and $^5D_1$ levels of f-f transitions of Eu^{3+} ions respectively. The Eu^{3+} ion has a CTB in the region of 200–300 nm.[39] Thus, excitation spectra exhibited a broad band around 280 nm which is attributed to the charge-transfer in the Eu^{3+}-O^{2-} species. The CTB of YAG:Eu^{3+} corresponds to the electronic transition from 2p orbital of O^{2-} to the 4f orbital of Eu^{3+}. With progress of heat-treatment the charge transfer band shifts towards higher energy side (blue shifting) due to the decreased covalency in the glass-ceramics compared to the mother glass. A similar type of CTB has also been reported in nano-sized YAG:Eu^{3+} particles by Nakamura et al.[36]

(8) Lifetime

Fig. 12 shows the room temperature fluorescence decay curves of Eu^{3+} ions in mother glass (a) and nano glass-ceramics (c and e) of the emission transition ($^5D_0 \rightarrow {}^7F_2$) at 613 nm with an excitation at 396 nm. The measured curves demonstrate a single exponential decay. The excited state lifetime (τ_f) for all has been estimated from these decay curves and the results are shown in Table II. It is seen that the excited state ($^5D_0$) lifetime (τ_f) increases with increase in Eu^{3+}:YAG nanocrystallite sizes. Such variation can be attributed to the high interaction of smaller particles with the high energy phonons of surrounding silicate glass (about 1100 cm^{-1}) which increases the nonradiative relaxation with decrease in particle size.[40] In larger particles, less interaction with surrounding glass along with stable crystal site occupation by the Eu^{3+} ion in the low phonon energy YAG host (about 690 cm^{-1} of YAG nanocrystal, see Fig. 8A) decrease the nonradiative relaxation[41] and thereby increase the measured lifetime (τ_f) as governed by the equation[42]

$$\tau_f = \frac{1}{\gamma_r + \gamma_{nr}} \qquad (4)$$

where γ_r and γ_{nr} are the radiative and nonradiative rates respectively. A similar behavior has been found in other nano glass-ceramics containing nanocrystals of $LiTaO_3$ and LaF_2 doped with Eu^{3+} and Er^{3+} respectively.[26, 41]

IV. Conclusions

The thermal, structural and optical properties of Eu_2O_3 doped transparent glass and nano glass-ceramics in the K_2O-SiO_2-Y_2O_3-Al_2O_3 system are demonstrated here. The results of XRD, TEM, FESEM, and FT-IRRS evidenced the formation of nanocrystalline YAG phase in the KSYA glass matrix. The nanocrystallite size of YAG has been evaluated from XRD, and found to vary in the range 35-45 nm. The FESEM image revealed that with progression of heat-treatment the glassy matrix initially phase-separated followed by crystallization. The appearance of Al-O and Y-O vibration bands in FTIR reflection spectra are also characteristics of YAG phase formation. In addition, the fluorescence spectra of nano glass-ceramics demonstrate that the Eu^{3+} ion enter into the YAG crystalline phase and takes nearly C_s point symmetry in the place of Y^{3+} sites. We believe that this work would create new avenues in the area of YAG nano glass-ceramics in particular and other glass-ceramics of very high temperature melting crystals in general.

Acknowledgements

The authors thank Dr. D. K. Bhattacharya, Acting Director of the institute for his kind permission to publish this paper. They thank Dr. R. Sen, Head, Glass Division, CGCRI for his encouragement to carry out this work. The authors would like to thank Dr. K. Annapurna and Dr. K. Biswas, Scientists, CGCRI for their help in recording the photoluminescence and refractive indices respectively. They thankfully acknowledge the RRCAT, Indore for DTA measurements, and XRD and Electron Microscope Division of this institute for recording XRD patterns and microscopic images respectively.

References

[1]B. H. King and J. W. Halloran, "Polycrystalline Yttrium Aluminum Garnet Fibers from Colloidal Sols," *J. Am. Ceram. Soc.*, **78**, 2141-2148 (1995).

[2]S. M. Sim, K. A. Keller, and T. I. Mah, "Phase Formation in Yttrium Aluminum Garnet Powders Synthesized by Chemical Methods," *J. Mater. Sci.*, **35**, 713–716 (2000).

[3]X. D. Zhang, H. Liu, W. He, J. Y. Wang, X. Li, and R. I. Boughton, "Synthesis of Monodisperse and Spherical YAG Nanopowder by a Mixed Solvothermal Method," *J. Alloys Compd.*, **372**, 300–303 (2004).

[4]Y. H. Zhou, J. Lin, M. Yu, S. M. Han, S. B. Wang, and H. J. Zhang, "Morphology Control and Luminescence Properties of YAG:Eu Phosphors Prepared by Spray Pyrolysis," *Mater. Res. Bull.*, **38**, 1289–1299 (2003).

[5]X. Li, H. Liu, J. Y. Wang, H. M. Cui, X. D. Zhang, and F. Han, "Preparation of YAG:Nd Nano-Sized Powder by Co-Precipitation Method," *Mater. Sci. Eng. A*, **379**, 347–350 (2004).

[6]R. A. Rodriguez, E. De la Rosa, L. A. Diaz-Torres, P. Salas, R. Melendrez, and M. Barboza-Flores, "Thermoluminescence Characterization of Tb^{3+} and Ce^{3+} Doped Nanocrystalline $Y_3Al_5O_{12}$ Exposed to X- and β-Ray Irradiation," *Opt. Mater.*, **27**, 293–299 (2004).

[7]Z. Wu, X. Zhang, W. He, Y. Du, N. Jia, and G. Xu, "Preparation of YAG:Ce Spherical Phase-Pure Particles by Solvo-Thermal Method and Their Photoluminescence," *J. Alloys. Compd.*, **468**, 571-574 (2009).

[8]S. Fujita, A. Sakamoto, and S. Tanabe, "Luminescence Characteristics of YAG Glass-Ceramic Phosphor for White LED," *IEEE Sel. Top. Quantum Electron.*, **14**, 1387-1391 (2008).

[9]G. Xia, S. Zhou, J. Zhang, and J. Xu, "Structural and Optical Properties of YAG:Ce^{3+} Phosphors by Sol-Gel Combustion Method," *J. Cryst. Growth*, **279**, 357-362 (2005).

[10]D. Boyer, G. B. Chadeyron, and R. Mahiou, "Structural and Optical Characterizations of YAG: Eu^{3+} Elaborated by the Sol-Gel Process," *Opt. Mater.*, **26**, 101-105 (2004).

[11]S. Nakamura, H. Yoshioka, Y. Matsubara, T. Ogawa, and S. Wada, "Efficient Tunable Yb:YAG Ceramic Laser," *Opt. Commun.*, **281**, 4411-4414 (2008).

[12]J. Lu, M. Prabhu, J. Song, C. Li, J. Xu, K. Ueda, A. A. Kaminskii, H. Yagi, and T. Yanagitani, "Optical Properties and Highly Efficient Laser Oscillation of Nd:YAG Ceramics," *Appl. Phys. B*, **71**, 469-473 (2000).

[13]B. R. Johnson and W. M. Kriven, "Crystallization Kinetics of Yttrium Aluminum Garnet ($Y_3Al_5O_{12}$)," *J. Mater. Res.*, **16**, 1795-1805 (2001).

[14]M. Nishi, S. Tanabe, K. Fujita, K. Hirao, and G. Pezzotti, "Phase-Selective Cathodoluminescence Spectroscopy of Er:YAG Glass-Ceramics," *Solid State. Commun.,* **132**, 19-23 (2004).

[15]P. Jander, "An Investigation of Novel Materials for Active Optical Devices," *Ph.D. Thesis*, Optoelectronics Research Centre, Faculty of Engineering and Applied Science, University of Southampton, UK, Dec. 2002.

[16]R.N. Bhargava, D. Gallagher, X. Hong, and A. Nurmikko, "Optical Properties of Manganese-Doped Nanocrystals of ZnS," *Phys. Rev. Lett.*, **72**, 416-419 (1994).

[17]G. Xia, S. Zhou, J. Zhang, S. Wang, Y. Liu, and J. Xu, "Sol–Gel Combustion Synthesis and Luminescent Properties of Nanocrystalline YAG:Eu^{3+} Phosphors," *J. Cryst. Growth*, **283**, 257–262 (2005).

[18]A. Tarafder, K. Annapurna, R. S. Chaliha, V. S. Tiwari, P. K. Gupta, and B. Karmakar, "Processing and Properties of Eu^{3+}:$LiTaO_3$ Transparent Glass-Ceramic Nanocomposites," *J. Am. Ceram. Soc.,* **92**, 1934-1939 (2009).

[19]R. S. Chaliha, K. Annapurna, A. Tarafder, V. S. Tiwari, P. K. Gupta, and B. Karmakar, "Luminescence and Dielectric Properties of Nano-Structured Eu^{3+}:K_2O-Nb_2O_5-SiO_2 Glass-Ceramics," *Solid State Sci.*, **11**, 1325–1332 (2009).

[20]A. Tarafder, K. Annapurna, R. S. Chaliha, V. S. Tiwari, P. K. Gupta, and B. Karmakar, "Nanostructuring and Fluorescence Properties of Eu^{3+}:$LiTaO_3$ in Li_2O-Ta_2O_5-SiO_2-Al_2O_3 Glass-Ceramics," *J. Mater. Sci.*, **44**, 4495–4498 (2009).

[21]D. E. Zelmon, D. L. Small, and R. Page, "Refractive-Index Measurements of Undoped Yttrium Aluminium Garnet from 0.4 to 5.0 μm," *Appl. Optics*, **37**, 4933-4935 (1998).

[22]B. D. Cullity, *Elements of X-Ray Diffraction*, 2nd Edition, pp. 101-2, Addison-Wesley Publishing Co., London, 1978.

[23]A. M. Hofmeister and K. R. Campbell, "Infrared Spectroscopy of Yttrium Aluminum, Yttrium Gallium, and Yttrium Iron Garnet," *J. Appl. Phys.,* **72**, 638-646 (1992).

[24]L. M. Seaverson, S. Q. Luo, P. L. Chien, and J. F. McClelland, "Carbonate Associated with Hydroxide Sol-Gel Processing of Yttria:An Infrared Spectroscopic Study,**"** *J. Am. Ceram. Soc.*, **69**, 423-429 (1986).

[25]P. Apte, H. Bruke, and H. Pickup, "Synthesis of Yttrium Aluminum Garnet by Reverse Strike Precipitation," *J. Mater. Res.*, **7**, 706-711 (1992).

[26]Q. Lu, W. Dong, H. Wang, and X. Wang, "A Novel Way to Synthesize Yttrium Aluminum Garnet from Metal–Inorganic Precursors," *J. Am. Ceram. Soc.,* **85**, 490-492 (2002).

[27]G. Fuxi, *Optical and Spectroscopic Properties of Glass*, pp. 18-61, Springer-Verlag, Berlin, 1992.

[28]W. T. Carnall, P. R. Fields, and K. Rajnak, "Electronic Energy Levels of the Trivalent Lanthanide Aquo Ions. Eu^{3+}," *J. Chem. Phys.*, **49**, 4450-4455 (1968).

[29]A. Ivankov, J. Seekamp, and W. Bauhofer, "Optical Properties of Eu^{3+}-Doped Zinc Borate Glasses," *J. Lumin.,* **121**, 123-131 (2006).

[30]G. H. Beall and D. A. Duke, *Glass-Ceramic Technology in Glass Science and Technology;* Vol. 1, p.403, Edited by D. R. Uhlmann and N. J. Kreidl, Academic Press, New York, 1983.

[31]G. H. Beall and D. A. Duke, "Transparent Glass-Ceramics," *J. Mater. Sci.,* **4**, 340-352 (1969).

[32]H. C. Van De Hulst, *Light Scattering by Small Particles,* Wiley, New York, 1957.

[33]K. Hirano, Y. Benino and T. Komatsu, "Rare Earth Doping into Optical Nonlinear Nanocrystalline Phase Transparent TeO_2-based Glass-Ceramics", *J. Phys. Chem. Solids*, **62**, 2075-2082 (2001).

[34]X. Li, H. Liu, J. Wang, H. Cui, X. Zhang and F. Han, "Preparation of YAG Nano-sized Powder by Co-precipitation Method", *Mater. Sci. Eng. A*, **379**, 347-350 (2004).

[35]S. Georgescu, A. M. Chinie, A. Stefan and O. Toma, "Effects of Thermal Treatment on the Luminescence of YAG:Eu Nanocrystals Synthesized by a Nitrate-Citrate Sol-Gel Method", *J. Optoelectron. Adv. Mater.*, **7**, 2985-2990 (2005).

[36]T. Nakamura, S. Yanagida and Y. Wada, "Preparation of Nano-sized YAG:Eu^{3+} Particles by a Microwave-Assisted Polyol Process and Their Luminescence Properties", *Res. Chem. Intermed.*, **32**, 331-339 (2006).

[37]K. Binnemans and C. Görller-Walrand, "Application of the Eu^{3+} Ion for Site Symmetry Determination", *J. Rare. Earth*, **14**, 173-180 (1996).

[38]A. D. Sontakke, A. Tarafder, K. Biswas, and K. Annapurna, "Sensitized Red Luminescence from Bi^{3+} Co-Doped Eu^{3+}:ZnO-B_2O_3 Glasses", *Physica B*, **404**, 3525-3529 (2009).

[39]M. Kusaba, N. Nakashima, Y. Izawa, C. Yamanaka, and W. Kawamura "Two-Photon Reduction of Eu^{3+} to Eu^{2+} via the f′← f Transitions in Methanol," *Chem. Phys. Lett.*, **221**, 407-411 (1994).

[40]R. S. Meltzer, W. M. Yen, H. Zheng, S. P. Feofilov, and M. J. Dejneka, "Relaxation between Closely Spaced Electronic Levels of Rare-Earth Ions Doped in Nanocrystals Embedded in Glass," *Phys. Rev. B*, **66,** 224202 1-6 (2002).

[41]Y. Yu, D. Chen, E. Ma, Y. Wang and Z. Hu, "Spectroscopic Properties of Nd^{3+} Doped Transparent Oxyfluoride Glass Ceramics", *Spectrochim. Acta Part A*, **67**, 709-713 (2007).

[42]R. Reisfeld and C. K. Jørgensen, *Lasers and Excited States of Rare Earths,* p.98, Springer-Verlag, Berlin, 1977.

Figure Captions

Fig. 1. DTA curve of Eu^{3+}:K_2O-SiO_2-Y_2O_3-Al_2O_3 mother glass powder.

Fig. 2. Dilatometric curve of Eu^{3+}:K_2O-SiO_2-Y_2O_3-Al_2O_3 mother glass.

Fig. 3. (Color online) Photograph of Eu^{3+}: YAG (a) mother glass and (b-e) nano glass-ceramics (thickness: 2 mm) obtained after heat-treatment for different duration at 750^0C laid over the writing to show their transparency (for details see Table II and Section III (1)).

Fig. 4. Variation of refractive indices (Cauchy fitted) of Eu^{3+}: YAG (a) mother glass and (d) nano glass-ceramics 30 h heat-treated at 750^0C as a function of wavelength.

Fig. 5. XRD patterns of the samples a-e (for details see Table II) and opaque YAG glass-ceramics obtained after heat-treating the mother glass at 940 and 980^0C for 10 h duration.

Fig. 6. Bright field TEM image of nano glass-ceramics (e) and inset shows the SAED pattern from the dotted encircled region (for details see Table II).

Fig. 7. FESEM images of samples (a) c and (b) e (for details see Table II).

Fig. 8. (A) FT-IRR spectra of the samples a-e (for details see Table II) and (B) variation of reflectivities at 475 and 690 cm^{-1} bands as a function of heat-treatment time at 750^0C.

Fig. 9. (Color online) Absorption spectra of (a) mother glass and (c-e) nano glass-ceramics (thickness: 2 mm, for details see Table II).

Fig. 10. (Color online) Visible fluorescence spectra (λ_{ex} = 396 nm) of Eu^{3+}: YAG (a) mother glass and (b-e) nano glass-ceramics (for details see Table II) obtained after heat-treatment for various duration (inset: deconvolution of $^5D_0 \rightarrow {}^7F_2$ transition of sample e).

Fig.11. (Color online) Excitation spectra of (a) mother glass and (e) nano glass-ceramics (for details see Table II).

Fig. 12. (Color online) Decay curves for the $^5D_0 \rightarrow {}^7F_2$ emission transition of Eu^{3+} ion at 613 nm under excitation at 396 nm of samples a, c, and e (for details see Table II).

Table I. Some Measured and Calculated Properties of Eu^{3+} Doped Mother Glass

Properties	Corresponding value
Average molecular weight, M_{av}	97.4
Density, ρ ($g.cm^{-3}$)	3.033
Refractive indices:	
n_F (at 486.1 nm)	1.6005
n_D (at 589.2 nm)	1.5930
n_C (at 656.3 nm)	1.5894
Abbe number (υ_D)	53
Dispersive power (υ_D^{-1})	0.02
Molar refractivity, R_M (cm^3)	10.88
Electronic polarizability, α (cm^3)	4.31×10^{-24}
Eu^{3+} ion concentration, $N_{Eu^{3+}}$ ($ions.cm^{-3}$)	1.87×10^{22}
Crystallization peaks, T_{p1} and T_{p2} (^0C)	940 and 971
CTE, α, (50-350^{0}C) x 10^{-7} K^{-1}	111
Glass transition temperature, T_g (^0C) (DTA)	821
Glass transition temperature, T_g (^0C) (Dil.)	819
Dilatometric softening temperature, T_d (^0C)	867

Table II. Measured Lifetime, Asymmetric Ratio and FT-IRRS Intensity of Mother Glass and Nano Glass-Ceramics

Sample Identity	Heat Treatment Time (h)	Lifetime, τ_f (ms)	Asymmetric Ratio, I_{ED}/I_{MD}	FT-IRRS[a] Intensity (I_{YAG})	
				690 cm^{-1}	475 cm^{-1}
a	0	1.224	5.109	14.69	31.82
b	3	1.244	4.895	16.40	33.98
c	10	1.272	4.821	17.68	37.93
d	30	1.317	4.265	16.88	42.18
e	50	1.476	3.593	20.13	47.35

[a]FT-IRRS, Fourier transformed infrared reflectance spectroscopy.

Figures

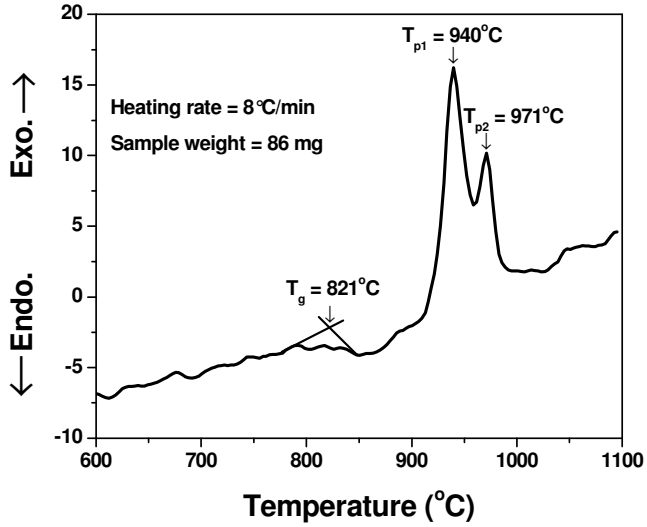

Fig. 1. DTA curve of Eu^{3+}:K_2O-SiO_2-Y_2O_3-Al_2O_3 mother glass powder.

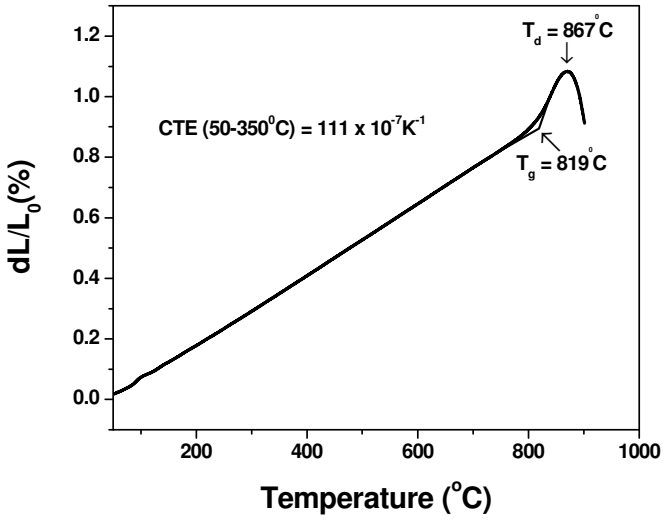

Fig. 2. Dilatometric curve of Eu^{3+}:K_2O-SiO_2-Y_2O_3-Al_2O_3 mother glass.

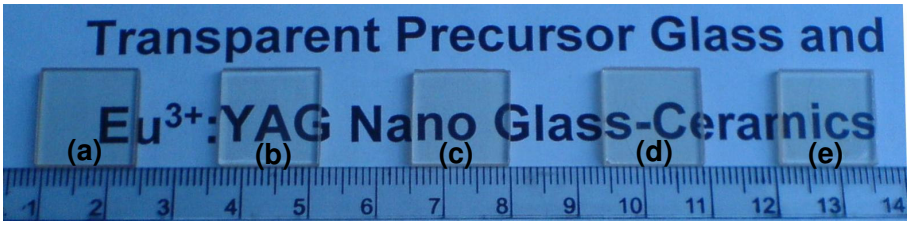

Fig. 3. (Color online) Photograph of Eu^{3+}: YAG (a) mother glass and (b-e) nano glass-ceramics (thickness: 2 mm) obtained after heat-treatment for different duration at 750^0C laid over the writing to show their transparency (for details see Table II and Section III (1)).

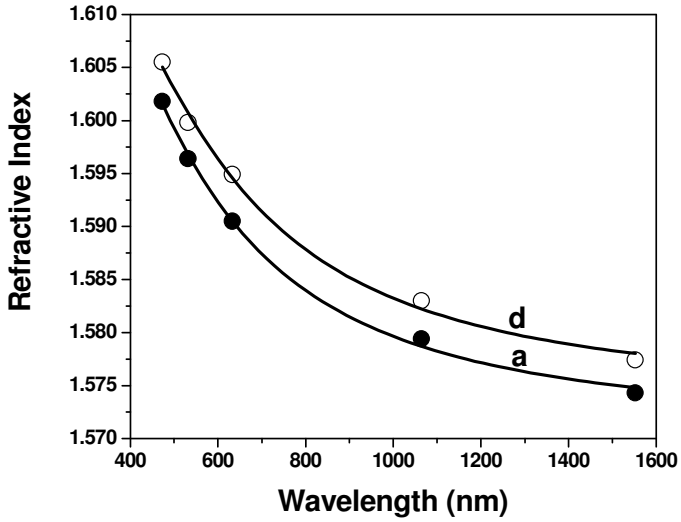

Fig. 4. Variation of refractive indices (Cauchy fitted) of Eu^{3+}: YAG (a) mother glass and (d) nano glass-ceramics 30 h heat-treated at 750^0C as a function of wavelength.

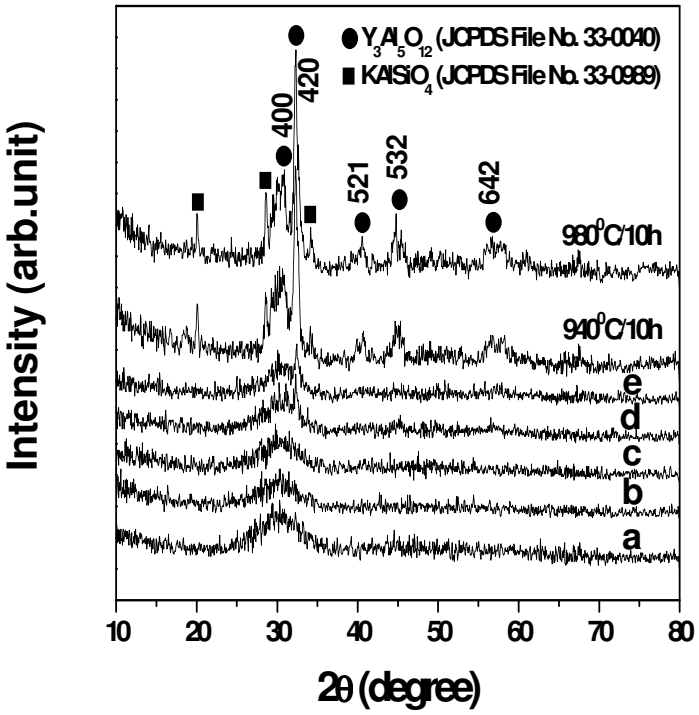

Fig. 5. XRD patterns of the samples a-e (for details see Table II) and opaque YAG glass-ceramics obtained after heat-treating the mother glass at 940 and 980^{0}C for 10 h duration.

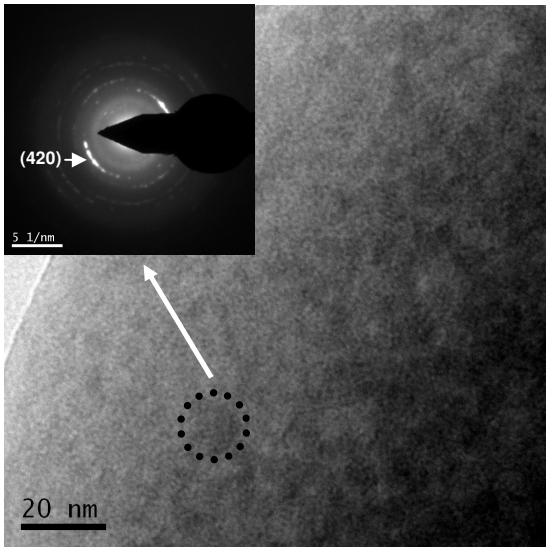

Fig. 6. Bright field TEM image of nano glass-ceramics (e) and inset shows the SAED pattern from the dotted encircled region (for details see Table II).

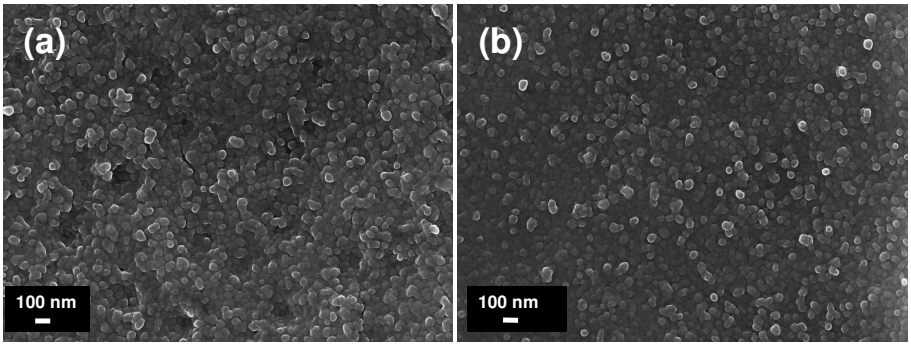

Fig. 7. FESEM images of samples (a) c and (b) e (for details see Table II).

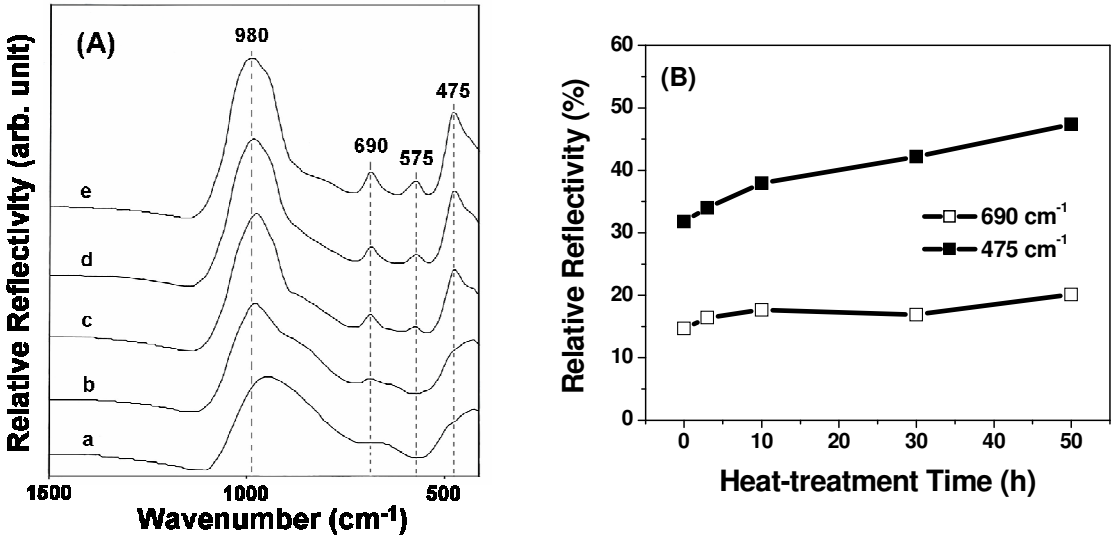

Fig. 8. (A) FT-IRR spectra of the samples a-e (for details see Table II) and (B) variation of reflectivities at 475 and 690 cm^{-1} bands as a function of heat-treatment time at 750^0C.

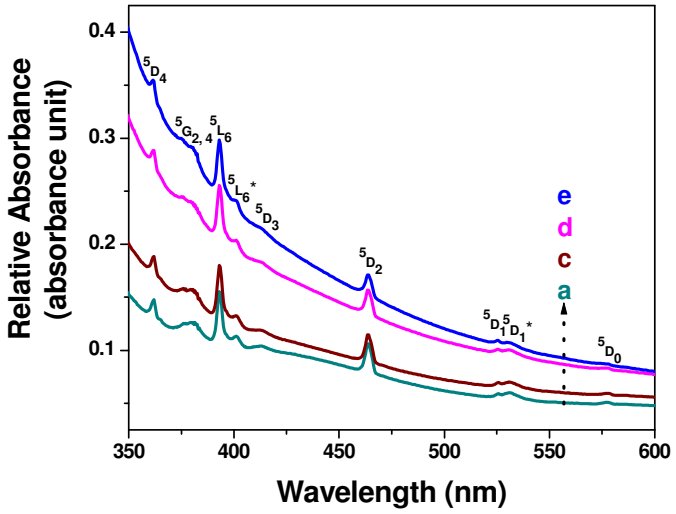

Fig. 9. (Color online) Absorption spectra of (a) mother glass and (c-e) nano glass-ceramics (thickness: 2 mm, for details see Table II).

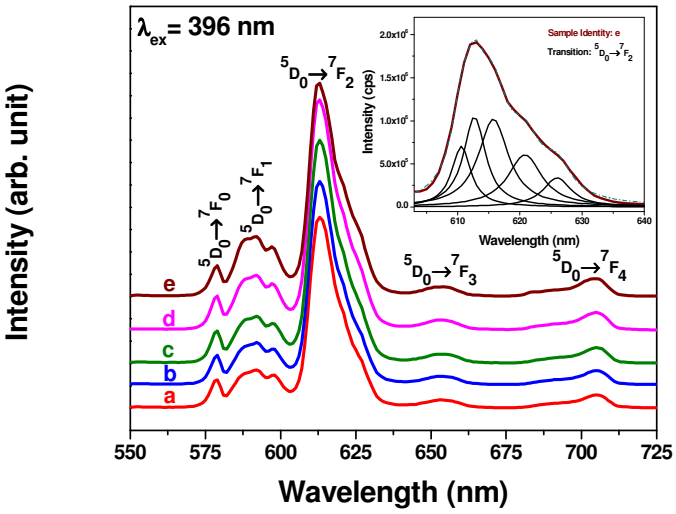

Fig. 10. (Color online) Visible fluorescence spectra (λ_{ex} = 396 nm) of Eu^{3+}: YAG (a) mother glass and (b-e) nano glass-ceramics (for details see Table II) obtained after heat-treatment for various duration (inset: deconvolution of $^5D_0 \rightarrow {}^7F_2$ transition of sample e).

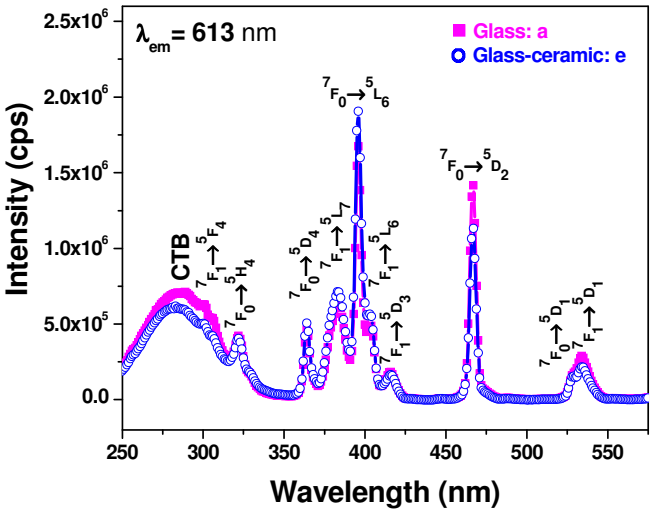

Fig.11. (Color online) Excitation spectra of (a) mother glass and (e) nano glass-ceramics (for details see Table II).

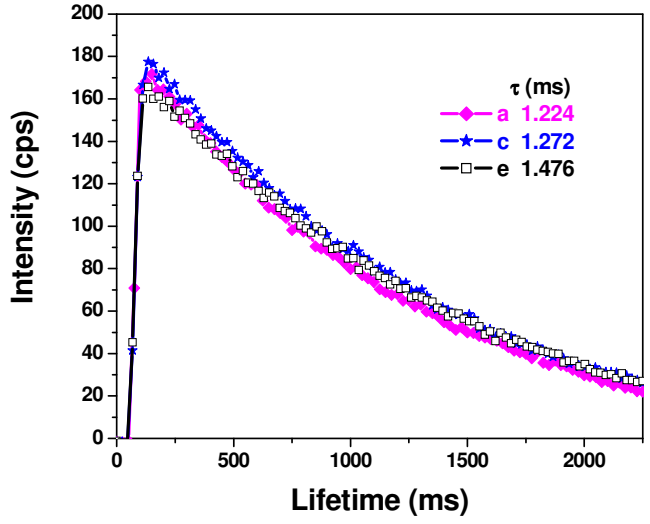

Fig. 12. (Color online) Decay curves for the $^5D_0 \rightarrow {}^7F_2$ emission transition of Eu^{3+} ion at 613 nm under excitation at 396 nm of samples a, c, and e (for details see Table II).